Model Optimization of Kinematic Redundant Feed Drive Systems Using Sailfish Optimization Algorithm

M. G. A. Nassef
Industrial and Manufacturing Engineering Department, Egypt-Japan University of Science and Technology, Alexandria, Egypt
Email: Mohamed.nassef@ejust.edu.eg

Taha Mostafa and Christian Schenck
Mechanical Engineering Department, Alexandria University, Alexandria, Egypt
Bremen institute for mechanical Engineering, University of Bremen, Bremen, Germany
Email: taha.mostafa@alexu.edu.eg, schenck@bime.de

***Abstract*—Kinematic redundant systems as part of machine tools reduce the dynamic requirements for feed axes and aim to increase the productivity. Yet, optimization of the system dynamic behaviour demands a deep understanding of how the dynamic coupling between the axes influences the tracking accuracy at the tool center point. This can be achieved through minimizing the discrepancies between the model output and physical measurements. One way is by optimizing the values of the dynamic coupling model parameters. In the present research, a heuristic algorithm, inspired by sailfish optimization algorithm, is developed to identify the stiffness and damping parameters of the investigated dynamic coupling model. Minimum RMS error is selected as the objective function parameter. Tests are conducted using different step and rectangular functions. Simulation results demonstrate the effectiveness of the proposed method to improve the model accuracy in simulating the vibrational response of kinematic redundant axes to jerk forces.**

***Index Terms*—kinematic redundancy, feed drive systems, sailfish optimization algorithm, jerk induced vibrations, dynamic coupling**

I. Introduction

Kinematic redundancy [1-3] presents a solution in the industry to enhance productivity and positioning accuracy of machine tools. An example of kinematic redundancy is a feed drive system consisting of two serially coupled axes that are moving independently in the same coordinate. One positive outcome is that the state of the tool center point (TCP) at any instant is the summation of the individual axes motion parameters. Early attempts in [4] to synchronize and coordinate the motion between the basic and the redundant axis used a dynamic approach rather than a pure geometric approach. The structure limitations such as singularities and limited effective workspace of the axis were overcome by using parallel redundant links [5] or in [6] by using hybrid kinematic structures.

jerk induced vibration [7] is a main phenomenon that arises during high dynamic motions. The reactive jerk forces, induced by the high-speed motion of one axis, are transmitted to the other axis and act as disturbances, which leads to undesired vibrations of the axis table. This hinders the possibility to fully exploit the advantages of kinematic redundancy in feed drive systems. This issue was addressed in [8] by developing a dynamic coupling model. The magnitude and frequency of the transmitted jerk forces from one axis to another is controlled by the values of stiffness and damping elements in the dynamic coupling model. However, inconsistency remained between the model output and measurements. This problem was attributed in [9] to a deviation of parameter values in the dynamic coupling model from the real system. The values of mechanical stiffness, viscous damping, and mass in the model were approximately calculated in [10, 11] based on the material and dimensions of coupling plate, fasteners, and axes mechanical parameters. Therefore, nonlinear identification of the parameters' values in the dynamic coupling model is of great interest.

The current work applies a framework using sailfish optimization algorithm (SFO) to determine the optimum model parameters. The criteria to be selected in the objective function is minimum RMS error. It is defined as the root mean square difference between the model output (undesired carrier axis displacement) and measurements. The results from the algorithm are compared with those before optimization [12] and with results from two optimization algorithms from literature: ant colony optimization (ACO) and particle swarm optimization (PSO) algorithms.

Manuscript received July 7, 2021; revised November 11, 2021.

doi: 10.18178/ijmerr.11.3.187-191

II. System Description

The current investigation was carried out on the kinematic redundant feed drive system shown in Fig. 1. The tested system specifications were described in [10] and it consisted of two ball screw mechanisms driven by permanent magnet AC servo actuators. The carried axis was mounted collinearly to the table of the carrier axis forming a kinematic redundant structure that supported the Tool Center Point (TCP). The motion of the TCP at any instant was equal to the summation of the individual motions of carried and carrier axes.

Fig. 2 shows a block diagram of the kinematic redundant system developed in Simulink. As both axes were allowed to move in one direction, the problem was reduced to a single degree of freedom system and the carried axis was excited in the direction of force. When the carried axis is commanded to move the TCP with a certain trajectory, a reaction force F1, equal in amplitude but opposite in the direction to the jerk force, is generated on the carried axis. The intermediate plate that holds the carried axis and is fixed to the nut of the carrier axis acted as a spring-damper system, and hence, it transmits a fraction of the induced forces to the carrier axis Ft1 resulting in an undesired displacement.

In this work, a set of experiments was formulated to test the dynamic reaction of the model under the influence of two main parameters: input command amplitude X and the velocity of an axis v. The levels of each motion parameter were selected in this work based on the effective workspace range of each axis and the maximum axes velocities, as shown in Table I.

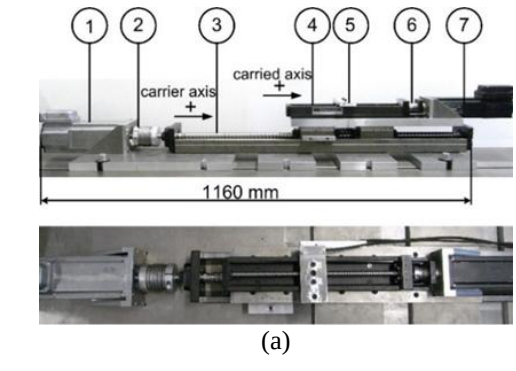

(a)

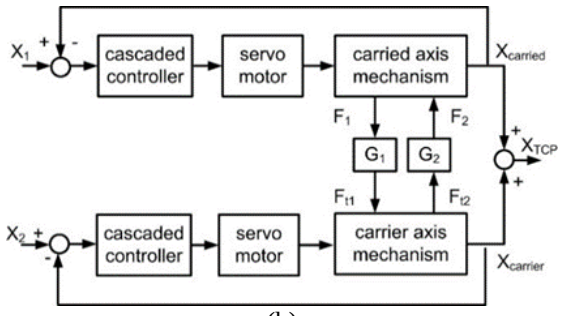

(b)

Figure 1. (a) the redundant structure assembly: 1, 7 two synchronous servomotors; 3,4 ball screws; 5 tool center point; 2, 6 flexible couplings, b) a simplified block diagram of the kinematic redundant feed drive system [10].

TABLE I. Carried Axis Step Command Tests And Their Parameter Values.

	Step Command Tests					
Parameter	A1	A2	A3	v1	v2	v3
X (mm)	1	0.75	0.5	1	1	1
v (mm/s)	500	500	500	500	400	250

III. Sailfish Optimization Algorithm

Sailfish optimization algorithm [12] is a recently developed heuristic algorithm to provide optimum solutions for complex stochastic problems. Its structure is developed based on the marine zoological behaviour of sailfish and sardine groups. When compared to other intelligent swarm algorithms, SFO showed competitive results in terms of exploration and exploitation phases. It also demonstrated high-speed convergence levels to reach global optimization, while avoiding local optima points. A description of sailfish optimization algorithm, used in this work, is presented as follows:

A. Initiation Phase

Sailfish and sardine positions are arbitrarily initiated according to the space area and constraints as:

$$X = \begin{bmatrix} X_{11} & X_{12} & \dots & X_{1j} \\ X_{21} & X_{22} & \dots & X_{2j} \\ . & . & . & . \\ . & . & . & . \\ . & . & . & . \\ X_{i1} & X_{i2} & \dots & X_{ij} \end{bmatrix} \quad Y = \begin{bmatrix} Y_{11} & Y_{12} & \dots & Y_{1j} \\ Y_{21} & Y_{22} & \dots & Y_{2j} \\ . & . & . & . \\ . & . & . & . \\ . & . & . & . \\ Y_{i1} & Y_{i2} & \dots & Y_{ij} \end{bmatrix} \tag{1}$$

Where X and Y represent the sailfish matrix and sardine matrix, respectively. i is the number of iteration loops. j refers to the number of the parameters of the dynamic coupling model in the matrix. Thus, X and Y matrices have the same number of columns (same number of parameters under investigation). In the initialization phase, sardine and sailfish agents are given random values for each parameter in the matrices for the search of the best fitness function in each iteration.

B. Finding the Elite Sailfish and Injured Sardine

The sailfish with the best fitness function is considered as the elite sailfish that is qualified for attack and injuring sardines. Furthermore, the elite sailfish does not update its position in the next iteration as far as the best solution has not been lost. On the other hand, the sardine with the best fitness function is called the injured sardine that is most exposed to be injured.

C. Adjusting Sailfish Positions

Equation (2) represents the modification method for positions based on the elite sailfish location and injured sardine.

$$X^{i+1} = X^{i}_{eli} - \gamma \times \left(\beta \frac{X^{i}_{eli} + Y^{i}_{inj}}{2} - X^{i} \right) \tag{2}$$

Where Xi+1 is the updated position of the Sailfish at i+1 iteration, Xelii is the actual elite sailfish, Yinji is the

actual injured Sardine, β is the random number (0 < β < 1). (γ) is a coefficient calculated at each update using (3).

$$\gamma = PD \times (2\beta - 1) \tag{3}$$

Where PD is the prey density and is calculated using (4).

$$PD = 1 - \frac{N_{sf}}{N_s + N_{sf}} \tag{4}$$

Where Nsf and Ns are the number of sailfish and sardine in each cycle, respectively. Adjusting Sardine Positions.

D. Adjusting Sardine Positions

Each sardine tends to escape and maneuver in accordance with (5):

$$Y^{i+1} = r \times \left(X_{eli}^{i} - Y^{i} + AP\right) \tag{5}$$

Where r is a random number (0 < r < 1)., AP clarifies the sailfish attack power at each iteration and is determined based on (6) as follows:

$$AP = A \times (1 - (2 \times itr \times \varepsilon)) \tag{6}$$

A and ε are coefficients that represents the decaying of the sailfish's attack power. On the other hand, itr is the number of iteration cycle. If AP > 0.5, all sardine groups will update their positions and if AP < 0.5, only (a) number of sardines will update their positions according to (7).

$$a = N_s \times AP \tag{7}$$

Each sardine will be killed if its fitness function is better than the sailfish's. In other words, the sardine will be killed if it will be in a better position for the sailfish to easily reach and hunt. Consequently, the sailfish will occupy the space of sardine (elite sailfish) and the sardine will be removed from the school. The number of sardines will be reduced according to (8) as follows:

$$X_i = Y_i \quad \text{if} \quad \text{fit}(Y_i) > \text{fit}(X_i) \tag{8}$$

E. Work Procedure

The present method relies on optimum selection of dynamic coupling model parameters by means of SFO and minimum RMS error as a fitness function. The procedure is explained in the following steps:

(i) Sailfish and sardine matrices are generated with random values of each parameter in the dynamic coupling model according to each parameter constraints.

(ii) In each iteration, the parameters of each agent are substituted in the model and the tested command is applied to carried axis model. The corresponding response signal of carrier axis signal is then recorded.

(iii) For each agent in the iteration, RMS error values are determined. The agent (sailfish or sardine) with the best fitness function is selected as the best position. In case the agent is sailfish (elite sailfish), it will remain in its position until next iteration, however, if the agent is sardine (injured sardine) then the sailfish agents will relocate their positions towards it.

(iv) The values of the agents are updated accordingly in the next iteration until the termination condition is reached (All sardines are killed, or number of iterations is reached).

IV. Results and Discussion

Fig. 2 illustrates the displacement of carrier axis obtained from measurements, simulation model based on the calculated values in [10], ACO, PSO, and using SFO algorithm for A1 test. A noticeable difference is observed between the results using calculated values and measurements in terms of signal amplitude (peak to peak) and damping (logarithmic decrement) parameters. Compared to measurements, results using calculated values deliver the highest peak to peak amplitude error in the first cycle of displacement reaching 27 % for A1, as shown in Fig. 3.

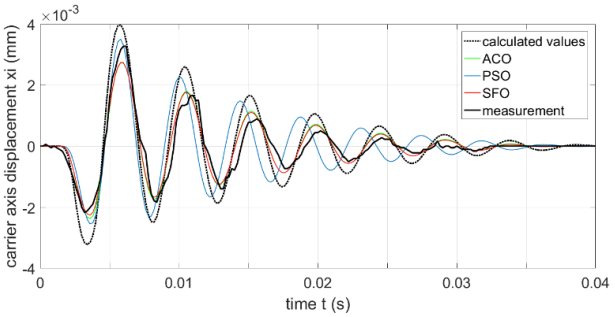

Figure 2. carrier axis displacement results for A1 step command test.

In comparison, simulation results from SFO algorithm deviates from measurement by only 4 %. The error values are 6% and 13% when using ACO and PSO algorithms, respectively. In case of tests A2 and A3, the results using calculated values showed significant deviation from measurements peaking at 59 % and 72 %, respectively. For those from ACO and PSO approaches, the peak-to-peak error reached only 9 % and 18 %, while in case of SFO, the peak-to-peak error is reduced to only 5%. Reducing the step size from A1 to A3 resulted in a proportional increase in the peak-to-peak error between the calculated values approach and measurements. This could be attributed to the increase of signal-to-noise (SNR) ratio of carrier axis displacement measurements at the submillimeter level. For tests v1, v2, and v3, the results from SFO, ACO, and PSO approaches remained unchanged settling down at around 1 %, while calculated values show greater peak to peak errors of around 27 % for v1, 44 % for v2, and 33 % for v3. Simulation signals from PSO, ACO and calculated values approaches featured the same frequency as the measured signal frequency (around 48 Hz). It can be seen that the damping error between measurements and SFO, ACO, and PSO was merely 4 % for all tests, while this value was around 15 % in case of calculated values approach. This indicates that the model response using SFO algorithm is better representing the disturbance response of the carrier axis under the effect of moving the carried axis at different step sizes and velocities.

For validation of results, a rectangular pulse function T1 was tested on the carried axis. The test function starts at 0 mm amplitude with a rise time of 0.002 s to reach the maximum amplitude of 5 mm then return back to 0 mm with a dwell time of 0 s. Fig. 4 shows the results obtained from both measurements and simulation from the four approaches. It can be seen that the SFO approach signal follows the measured signal better than the signals from other approaches.

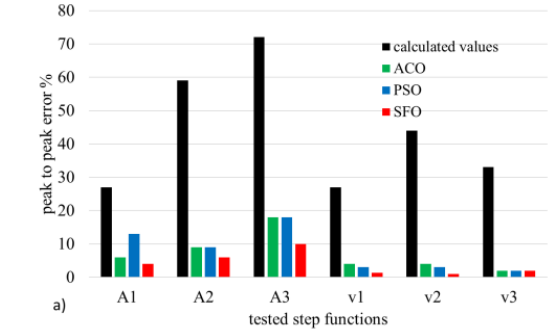

(a)

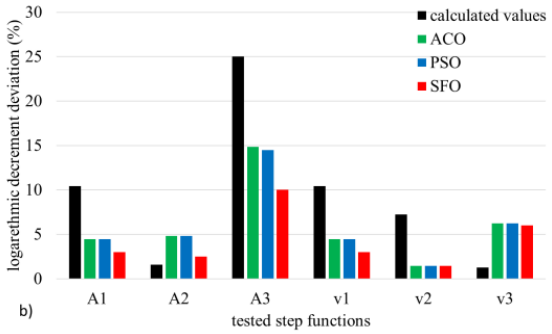

(b)

Figure 3. the difference between measurements and simulation outputs for all tested step functions in terms of a) peak to peak error, and b) damping deviation.

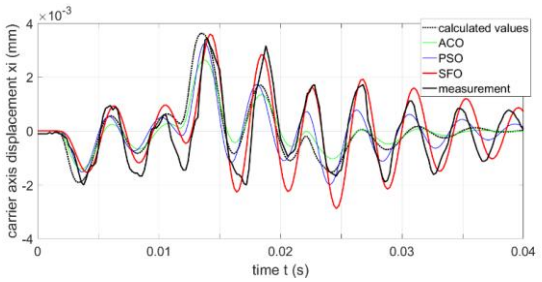

Figure 4. carrier axis displacement results for tests T1.

The frequency components and their energy contents of simulation signals were also determined and compared with measurement using power spectrum density (PSD). Fig. 5 shows the power spectrum density results for test T1. By comparing signals and their power spectral densities, it is noticed that measurement signal for T1 has three components at 44 Hz, 156 Hz, and 244 Hz. Simulation results from the four approaches are found to have the same frequency components as measurements with an error margin at each frequency of around 9 %, 2 %, and 5 %, respectively.

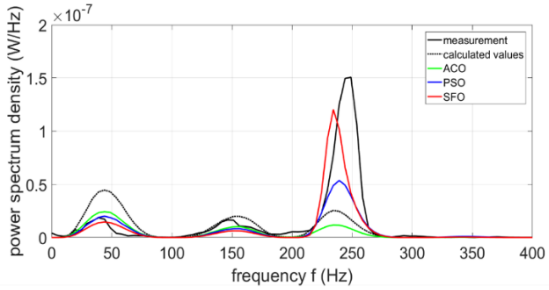

(a)

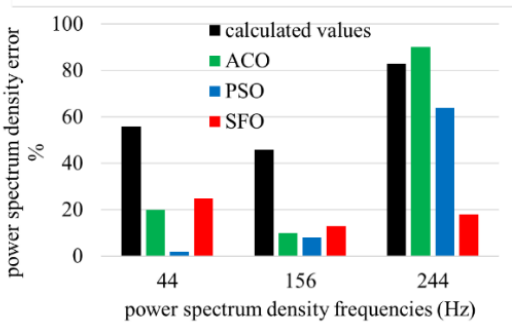

(b)

Figure 5. a) power spectrum density of simulation results and measurement and b) corresponding power spectral density error at each frequency.

The energy content at the first frequency component showed a significant deviation in case of calculated values approach of 56 % from measurement. This value is around 46 % and 83 % for the second and third frequency components. In case of SFO and these values were 25 %, 12 %, and 18 %, which are lower than those of PSO and ACO.

V. Conclusions

Kinematic redundancy is a promising solution to increase the productivity of high-speed machine tools. However, induced vibrations in axis during high dynamic motions require deep understanding of how these vibrations are transmitted in the structure coupling between axes. Therefore, simulation model of the redundant axes requires parameter optimizing of the dynamic coupling model using sailfish optimization algorithm. The deviation between the model output and measurements has been compared by calculating peak-to-peak error, frequency, and damping deviation for simple step functions. The identified parameter values in the case of SFO are found to reduce the discrepancies between simulation and experimental results. Validation of work was conducted on a rectangular function. Power spectra and frequency correlation were determined, and the results showed good potential of SFO in following the measurement signals.

Conflict of Interest

This research has received no external funding. The authors declare no conflict of interest or competing interest in this research.

AUTHOR CONTRIBUTIONS

M G A Nassef and Christian Schenck conducted the experimental research; M G Nassef analyzed the data and developed the simulation model; Taha Mostafa developed and verified the heuristic optimization algorithms, M G A Nassef and Taha Mostafa prepared the original draft of the paper; Christian Schenck reviewed and edited the final paper; all authors had approved the final version.

REFERENCES

[1] B. Gonul, O. F. Sapmaz, and L. T. Tunc, "Improved stable conditions in robotic milling by kinematic redundancy," *Procedia CIRP*, vol. 82, pp. 485-490, 2019.

[2] D. Zhang, Y. Xu, J. Yao, B. Hu, and Y. Zhao, "Kinematics, dynamics and stiffness analysis of a novel 3-DOF kinematically/actuation redundant planar parallel mechanism," *Mechanism and Machine Theory*, vol. 116, pp. 203-216, 2017.

[3] Y. Jiang, T. Li, L. Wang, and F. Chen, "Improving tracking accuracy of a novel 3-DOF redundant planar parallel kinematic machine," *Mechanism and Machine Theory*, vol. 119, pp. 198-218, 2018.

[4] B. Kuhfuss and C. Schenck, "Diversion of tool paths in kinematic redundant machining: A general approach for different design requirements," *WGP-Annals Production Engineering*, vol. XIII, pp. 197 – 202, 2006.

[5] L. T. Schreiber and C. Gosselin, "Kinematically redundant planar parallel mechanisms: Kinematics, workspace and trajectory planning, *Mechanism and Machine Theory*, vol. 119, pp. 91-105, 2018.

[6] H. Ye, D. Wang, J. Wu, Y. Yue, and Y. L. Zhou, "Forward and inverse kinematics of a 5-DOF hybrid robot for composite material machining," *Robotics and Computer-Integrated Manufacturing*, vol. 65, 2020.

[7] R. Sato and K. Shirase, "Analytical time constant design for jerk-limited acceleration profiles to minimize residual vibration after positioning operation in NC machine tools," *Precision Engineering*, vol. 71, pp. 47-56, 2021.

[8] M. G. A. Nassef, C. Schenck, and B. Kuhfuss, "Compensation of induced vibrations by commanded counter motions in kinematic redundant feed drive systems," in *Proc. 10th IEEE International Conference on Control and Automation (ICCA)*, China, 2013, pp. 1497-1502.

[9] M. G. A. Nassef, C. Schenck, and B. Kuhfuss, "Simulation-based parameter identification of a reduced model using neural networks," in *Proc. 9th IEEE International Conference on Control and Automation (ICCA)*, Chile, 2011, pp. 974-978.

[10] M. G. A. Nassef, "Dynamic behavior of kinematic redundant actuators in feed drive systems," Ph.D. thesis, Bremen institute for mechanical engineering bime, FB04, University of Bremen, 2013.

[11] T. Sun and B. Lian, "Stiffness and mass optimization of parallel kinematic machine," *Mechanism and Machine Theory*, vol. 120, pp. 73-88, 2018.

[12] S. Shadravan, H. Naji, and V. K. Bardsiri, "The sailfish optimizer: a novel nature-inspired metaheuristic algorithm for solving constrained engineering optimization problems," *Engineering Applications of Artificial Intelligence*, vol. 80, pp. 20-34, 2019.

M G A Nassef is born in Alexandria, Egypt in Feb 1984. He received his B.Sc. and M.Sc. degrees from the Production Engineering Department at Alexandria University in Egypt. Afterwards, he was awarded a fully funded scholarship from the German academic exchange services (DAAD) to pursue his Ph.D. degree in production engineering from the University of Bremen. He obtained his degree in the field of machine tool dynamics and control from Bremen institute for mechanical engineering (bime). Between 2014 and 2019, he joined Alexandria University as an assistant professor teaching manufacturing and mechanical engineering courses for undergraduates besides providing consultation services in industry in the field of fault diagnosis of machinery.

He is currently holding a position of Associate professor and acting chairperson of the industrial and manufacturing engineering (IME) department at Egypt-Japan University of Science and Technology. He leads a research group involved in two main tracks: fault diagnosis of rotating machinery and dynamic characterization of composite materials. His research topics includes early fault detection and diagnosis of rolling bearings and manufacturing and characterization of natural fiber composites for industrial applications. His expertise covers the application of advanced signal processing techniques, vibrations measurement and analysis, heuristic algorithms, modeling and simulation, and experimental modal analysis technique. He is a reviewer for many scientific journals in the field of his expertise.